nanomaterials

MDPI

Article

An Improved Smart Meta-Superconductor MgB_2

Xiaopeng Zhao *, Qingyu Hai, Miao Shi, Honggang Chen, Yongbo Li and Yao Qi

Smart Materials Laboratory, Department of Applied Physics, Northwestern Polytechnical University, Xi'an 710129, China; haiqingyu@mail.nwpu.edu.cn (Q.H.); shimiao@mail.nwpu.edu.cn (M.S.); 2017100698@mail.nwpu.edu.cn (H.C.); 2014100616@mail.nwpu.edu.cn (Y.L.); qiyao@mail.nwpu.edu.cn (Y.Q.)
* Correspondence: xpzhao@nwpu.edu.cn

Abstract: Increasing and improving the critical transition temperature (T_C), current density (J_C) and the Meissner effect (H_C) of conventional superconductors are the most important problems in superconductivity research, but progress has been slow for many years. In this study, by introducing the p-n junction nanostructured electroluminescent inhomogeneous phase with a red wavelength to realize energy injection, we found the improved property of smart meta-superconductors MgB_2, the critical transition temperature T_C increases by 0.8 K, the current density J_C increases by 37%, and the diamagnetism of the Meissner effect H_C also significantly improved, compared with pure MgB_2. Compared with the previous yttrium oxide inhomogeneous phase, the p-n junction has a higher luminescence intensity, a longer stable life and simpler external field requirements. The coupling between superconducting electrons and surface plasmon polaritons may be explained by this phenomenon. The realization of smart meta-superconductor by the electroluminescent inhomogeneous phase provides a new way to improve the performance of superconductors.

Keywords: smart meta-superconductor; p-n junction nanostructured inhomogeneous phase; electroluminescent; injecting energy; electron-surface plasmon polaritons coupling; smart superconductivity

Citation: Zhao, X.; Hai, Q.; Shi, M.; Chen, H.; Li, Y.; Qi, Y. An Improved Smart Meta-Superconductor MgB_2. *Nanomaterials* **2022**, *12*, 2590. https://doi.org/10.3390/nano12152590

Academic Editor: Yassine Slimani

Received: 8 July 2022
Accepted: 26 July 2022
Published: 28 July 2022

1. Introduction

Superconductivity has greatly promoted the progress of industrial technology since its discovery, and has also expanded people's understanding of condensed matter physics [1]. The superconducting materials have a wide range of applications, such as electric grids [2], and quantum computing devices [3,4]. The pursuit of superconducting materials with a high critical temperature Tc has been promoting the research. The high-temperature superconductor [5,6], iron-based superconductor [7,8], high-pressure superconductor [9–12] and photoinduced superconductor [13,14] have been gradually studied and discovered. Superconductors have zero resistance characteristics and complete diamagnetism (the Meissner effect) [15–17]. Therefore, the transition from a superconducting state to a non-superconducting state has characteristic parameters: critical transition temperature (T_C), critical current density (J_C) and critical magnetic field (H_C) [15,18]. In recent years, it has been found that the superconductivity of the sulfur hydride system is 203 K at 155 GPa [9], and the carbonized sulfur hydride system is 287.7 K at 267 GPa [12]. Although this method can achieve higher superconducting transition temperatures and even room temperature superconductivity, the extremely high pressure and small sample size limit its further applications.

The discovery of the MgB_2 superconductor [19] has aroused great interest in the scientific community due to its excellent superconductivity and simple preparation process, especially its high T_C. In order to improve the superconductivity of MgB_2, various methods have been adopted [20–24], which can not only improve the practical application of MgB_2, but also further clarify its superconductivity mechanism. Chemical doping is often used to study superconductivity. Unfortunately, many experimental results have

confirmed that this approach reduces the T_C of MgB_2 [25–28]. So far, there is no effective strategy to improve the T_C of MgB_2. Chemical doping is the simplest method to change the J_C of the superconductor. Doping graphene in MgB_2 [29], and Al_2O_3 [30] and MgO [31] in BiSrCaCuO will reduce J_C under a zero magnetic field. At the same time, adding anthracene into MgB_2 [32] and Cr_2O_3 into BiSrCaCuO [33] will increase the J_C under a zero magnetic field. Under a zero magnetic field, chemical doping increases or decreases J_C of the superconductor, but correspondingly decreases T_C. There is no particularly effective method to increase T_C and J_C at the same time.

Metamaterials with artificial structures have supernormal physical properties [34,35]. With the development of metamaterials, researchers proposed that a metamaterial superconductor can exhibit a higher T_C [36–38]. In 2007, we proposed to introduce inorganic ZnO electroluminescent (EL) material into a Bi(Pb)SrCaCuO superconductor at a high temperature in order to affect its superconducting transition temperature [39,40]. In recent years, MgB_2 and Bi(Pb)SrCaCuO smart meta-superconductors (SMSCs) have been constructed. We doped Y_2O_3:Eu^{3+} and Y_2O_3:Eu^{3+}+Ag EL materials in conventional MgB_2 and high temperature Bi(Pb)SrCaCuO superconductors to form a smart meta-superconductor [39–47]. When the *Tc* of SMSCs is measured by the four-probe method, the external electric field can stimulate the inhomogeneous phase to produce EL, which can achieve the purpose of strengthening the Cooper pair and lead to the macroscopic change of *Tc*. SMSCs is a material that can adjust and improve *Tc* through external field stimulation, which is a new property that cannot be achieved by traditional second phase doping [44–46]. We believe that this is because superconducting particles acting as microelectrodes excite the inhomogeneous phase EL under the action of an applied electric field, and the energy injection promotes the formation of electron pairs. Recently, J_C and the Meissner effects of the MgB_2 and Bi(Pb)SrCaCuO smart meta-superconductors have been investigated [47]. The addition of Y_2O_3:Eu^{3+} and Y_2O_3:Eu^{3+}+Ag increased the J_C of MgB_2 and Bi(Pb)SrCaCuO, and indicating the Meissner effect at higher temperatures. It has been confirmed that the rare earth oxide inhomogeneous phase can improve the *Tc*, J_C, and Meissner effect of conventional and high temperature oxide superconductors. However, it is very difficult to improve the electroluminescence intensity, short luminescence life, large applied electric field and other factors of rare earth oxides, which limits the improvement of its superconducting performance.

In this paper, the smart superconductivity of MgB_2 was studied by introducing the p-n junction electroluminescence inhomogeneous phase to realize energy injection and improve electron pairing. Studies show that the high luminescence intensity and long life of the p-n junction nanostructure can ensure the stability of material properties. In addition, the p-n junction nanostructure excitation is easier, with only a few volts of excitation required rather than hundreds or even thousands of volts. Thus, the electric field applied by the four-point method for measuring superconductivity can be satisfied. Because the p-n junction nanostructured inhomogeneous phase exhibits good behavior under field excitation, the optimum amount of the inhomogeneous phase increased from 0.5wt.% to 1.0wt.% compared to oxide. Therefore, the critical temperature *Tc*, current density *Jc* and the Meissner effect of superconducting transition are higher than those of the oxide inhomogeneous phase. In particular, the performance stability of the material has been greatly improved, and can be stable for more than several hundred hours. We hold the opinion that the photons generated by the inhomogeneous phase of the p-n junction nanostructure interact with some superconducting electrons to generate surface plasmon polaritons (SPPs) and promote electron pair transport.

2. Model

Figure 1 shows the MgB_2 SMSCs model constructed with polycrystalline MgB_2 as raw material. The gray polyhedrons are polycrystalline MgB_2 particles, Φ is the particle size of MgB_2 particle, which will be described in detail in the experimental part. The red particles are p-n junction particles with red light wavelengths, which are dispersed

among MgB_2 particles as the inhomogeneous phase. The introduction of the inhomogeneous phase inevitably reduces the *Tc* of MgB_2, mainly because the doped inhomogeneous phase is not a superconductor, which is detrimental to the superconductivity of MgB_2, such as the MgO impurity phase in MgB_2. For convenience, the reduction of *Tc* after the introduction of the inhomogeneous phases is called the impurity effect [39–41]. The incorporation of inhomogeneous phases has been proved to be an effective method to improve T_C in MgB_2 and Bi(Pb)SrCaCuO systems. For example, the introduction of electroluminescence Y_2O_3:Eu^{3+} and Y_2O_3:Eu^{3+}+Ag can produce an electroluminescence effect and increase *Tc* [42–46]. There is obvious competition between the impurity effect and the EL excitation effect of the inhomogeneous phase. When the EL excitation effect is dominant, *Tc* is improved ($\Delta Tc > 0$). Otherwise, the inhomogeneous phase is introduced to reduce *Tc* ($\Delta Tc < 0$). Therefore, the impurity effect should be reduced as much as possible and the EL excitation effect should be enhanced in order to obtain high *Tc* samples. The superconductivity of a smart meta-superconductor can be improved and adjusted by adding the EL inhomogeneous phase [45,46]. It has been known that variations in *Tc* are often related to variations in electron density [48,49]. However, under the current preparation conditions, the inhomogeneous phase only exists between MgB_2 particles and does not react with MgB_2. Moreover, the diffusion between the inhomogeneous phase and MgB_2 particles is difficult, and the electron density cannot be significantly changed. Therefore, electron density is not a key tuning parameter affecting *Tc* variation. During the measurement process, the applied electric field forms a local electric field in the superconductor and excites the inhomogeneous phase to generate EL excited photon injection energy, which is beneficial to the enhancement of the Cooper pair and the change of *Tc*. However, given that photons may destroy the Cooper pair, the mechanism for the occurrence of *Tc* changes needs to be further explored. Later, according to the experimental results, we will explain this phenomenon by the inhomogeneous phase EL.

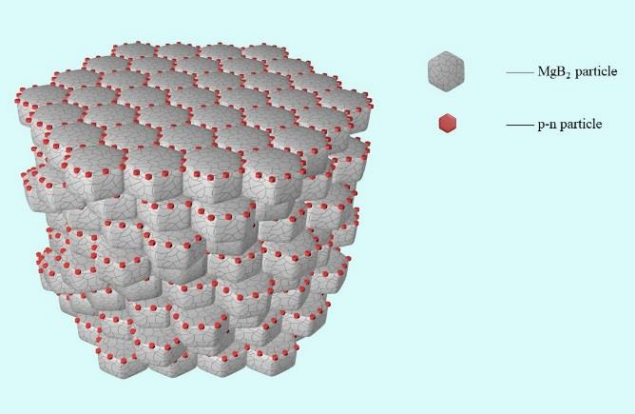

Figure 1. MgB_2 SMSCs model diagram.

3. Experiment

3.1. Preparation of p-n Junction Luminescent Particles

We purchased commercial red LED epitaxial chip, its luminous composition is the AlGaInP composite structure, and luminous wavelength is 623 nm. The compound AlGaInP is produced by Shandong Huaguang Optoelectronics Co., LTD., Jinan, China. It uses trimethylgallium, trimethylindium, trimethylaluminum and phosphorane as raw materials and as reactants, which are brought into the vacuum furnace by hydrogen for reaction growth on the substrate. The melting point of the product AlGaInP is between 1200 and 1400 °C. We stripped compounds off the substrate, ground them to obtain particles of about 4 μm × 4 μm × 1.7 μm. The particles consisted of three-layer nanostructures: a p-type semiconductor layer (250 nm thick), an active layer (250 nm thick), and an n-type semiconductor layer (1200 nm thick). The electroluminescence test method is the

same as that of rare earth luminescent particles, and the measurement conditions were given in the text. The applied voltage <10 V, current <10 mA, test luminescence curve is shown in Figure 2. The luminescence curves of the electroluminescent rare earth oxide particles in the figure were obtained from the samples prepared by our group [50,51]. It can be seen that the luminescence intensity of the p-n junction particles is much higher than that of electroluminescent rare earth oxide particles. After more than 2000 h of work, the luminescence intensity almost did not decay, and the luminescence behavior did not change after 100 days. The characteristics of high strength and long life of the p-n junction provided a solid foundation for improving smart meta-superconductors.

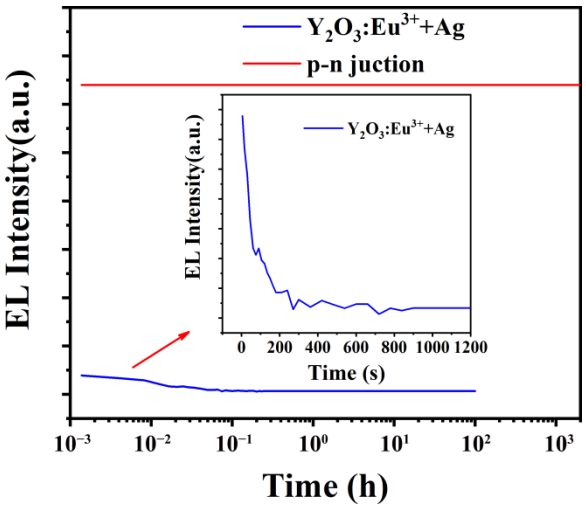

Figure 2. Luminescence intensity and lifetime test curves of p-n junction particles and rare earth oxide particles in red light wavelengths.

3.2. Preparation of MgB_2 Superconductor and Inhomogeneous Phase Samples

Magnesium diboride (MgB_2) was purchased from Alfa Aesar with a purity of 99% and a particle size of 100 mesh (150 μm). A certain amount of MgB_2 basic powder raw material was put into a 500 mesh (30 μm) stainless steel standard sieve, and the large sized particles were removed by screening to get the basic uniform size of MgB_2 particles, with a diameter of $\Phi \leq 30$ μm. Figure 3a,b show the SEM image of MgB_2 and the p-n junction particles. Figure 3c show the XRD test curves of pure MgB_2, AlGaInP and MgB_2+ 1.2 wt. % AlGaInP samples. Figure 3d is a partial enlarged drawing of Figure 3c, where the vertical dotted line corresponds to the diffraction peak of AlGaInP. The comparison results show that in addition to the MgB_2 phase, there is an independent AlGaInP phase in the doped sample, indicating that there is no chemical reaction between the two. A certain amount of MgB_2 powder raw materials and corresponding inhomogeneous phase p-n particles with different mass fractions were weighed and put into two beakers, respectively, to make an alcohol solution and then ultrasonic was used for 20 min. The two solutions were placed on a magnetic stirrer for stirring, and the inhomogeneous phase solution was added to the MgB_2 solution drop by drop during stirring. After the dripping, the mixed solution was stirred for 10 min and ultrasonic was used for 20 min. Then, it was transferred to petri dishes and dried in a vacuum drying oven at 60 °C for 4 h to obtain a black powder. The powder was fully ground and pressed into a wafer with a diameter of 11 mm and a thickness of 1.2 mm. The pressure and holding time were 14 MPa and 10 min, respectively. The wafer was then placed in a small box made of tantalum, and the box was then placed in an alumina porcelain boat, which was finally transferred to a vacuum tube furnace. In the high pure Ar atmosphere, the samples were slowly heated to 840 °C in the vacuum tube furnace for 10 min, then cooled to a 650 °C temperature calcination for 1h, and then slowly cooled to room temperature to obtain the corresponding samples [43,46]. Pure MgB_2 samples (represented by S0) and the p-n junc-

tion doped MgB_2 samples were prepared, with the concentration of dopant corresponding to each sample as shown in Table 1. In the experiment, the influence of the inhomogeneous phase of luminescence on the superconducting transition temperature of the MgB_2-based superconductor was studied by changing the content of the inhomogeneous phase.

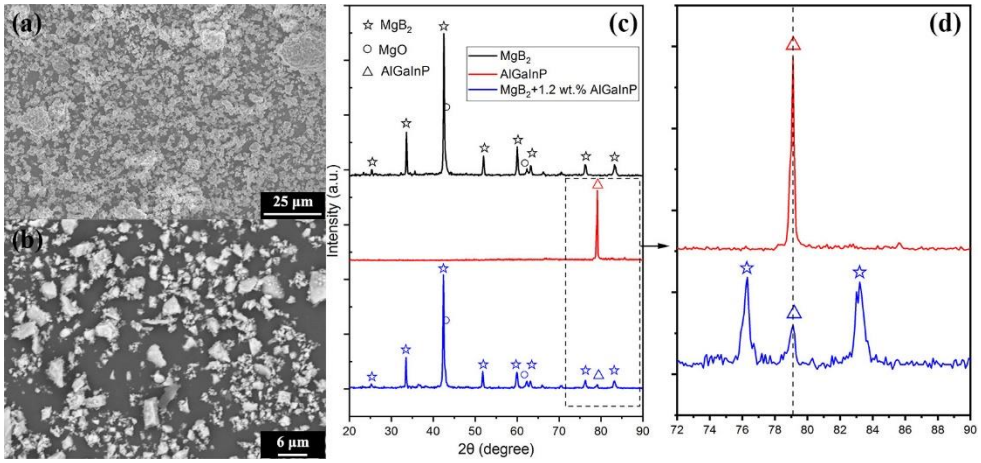

Figure 3. SEM diagram of (**a**) MgB_2 particles, diameter $\Phi \leq 30$ μm, (**b**) p-n junction particles, ground into 4 μm × 4 μm × 1.7 μm particles, (**c**) the XRD test curves of pure MgB_2, AlGaInP and MgB_2 + 1.2 wt. % AlGaInP samples, (**d**) a partial enlarged drawing of (**c**).

Table 1. MgB_2 doped inhoumgenous phase with different concentrations.

Sample	S0	S1	S2	S3	S4	S5	S6
Inhomogeneous phase p-n junction concentration (wt.%)	0	0.5	0.8	0.9	1.0	1.2	1.5

Figure 4a shows the SEM image of the MgB_2 + 0.9 wt.% p-n junction after sintering. Figure 4b–d show the EDS mapping for elements Mg, Al, and Ga listed in the top right corner of each figure. The distribution of elements in Figure 4 shows the discrete distribution of the Al and Ga elements and the aggregation distribution of the AlGaInP inhomogeneous phase. Due to the uneven size and distribution of the AlGaInP particles, as well as the distribution of Al and Ga elements in the particles during the p-n junction, preparation by vapor deposition may lead to the change of their positions and concentrations.

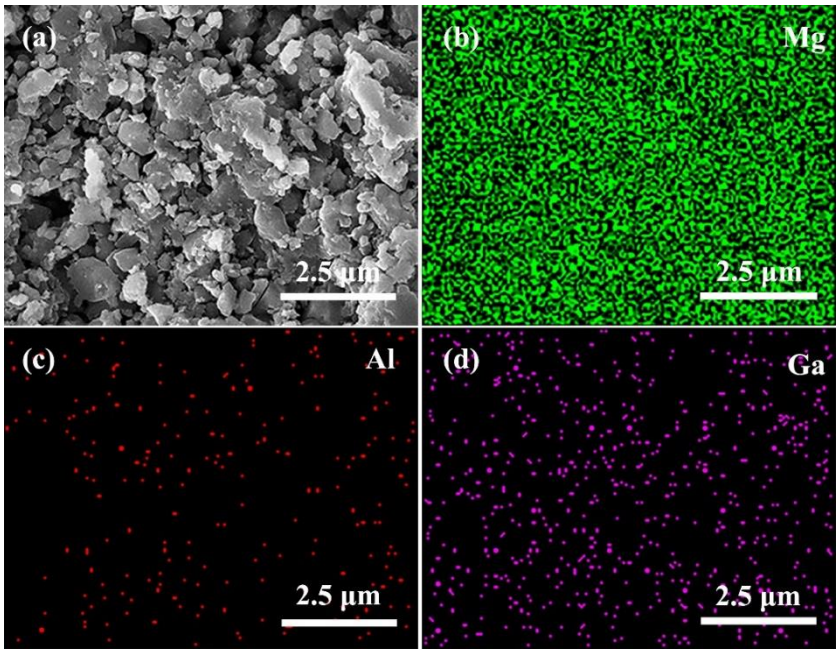

Figure 4. (**a**) SEM diagram of sample after sintering, (**b**–**d**) EDS mapping of Mg, Al, Ga.

3.3. Critical Transition Temperature Measurement

A four-lead method was used to measure the *R-T* curve of the sample at a low temperature, with a distance of 1 mm between the four probes to determine the superconducting transition temperature T_C of the sample. The closed-cycle cryostat manufactured by Advanced Research Systems provides a low temperature environment (the minimum temperature is 10 K); the test current (1–100 mA) is provided by the high temperature superconducting material characteristic test device, produced by the Shanghai Qianfeng Electronic Instrument Co., LTD., Shanghai, China, Voltages were measured using a Keithley nanovolt meter; we adjusted the test temperature with a Lake Shore cryogenic temperature controller. The whole testing process was carried out in a vacuum environment [41,46].

3.4. Measurement of Critical Current Density and Meissner Effect

The sample was placed in a low-temperature medium and the current-voltage (*I-V*) characteristic curve was measured by a four-probe method under a zero magnetic field. A certain amount of direct current was connected to the prepared sample by two leads, and the other two leads were used to measure the voltage of the prepared sample by a Keithley digital nanovoltmeter. We used indium wire to connect the sample to the lead, and the distance between the two voltage leads for all samples is 1 mm. When the current *I* passing through the sample exceeds a certain value, the superconducting state is destroyed and changes to the normal state. This current is called the critical transport current of the superconductor. Typically in superconducting systems, the transport critical current density (J_C) is determined by *I-V* measurements at different temperatures (below the initial transition temperature $T_{C,on}$), with a voltage criterion of 1 μV/cm [47,52–54]. The shape and size of all samples and the distance between the current and voltage leads were kept the same during the test. Subsequently, the prepared samples were tested for DC magnetization [47,55]. The samples were cooled slowly in a magnetic field of 1.8 mT parallel to the plane, and data were collected during heating. All samples showed complete diamagnetism.

4. Results and Discussion

Figure 5 is the normalized resistivity curve of the doped x wt.% luminescent inhomogeneous phase p-n junction (x = 0, 0.5, 0.8, 0.9, 1.0, 1.2, 1.5) prepared with MgB_2 raw material. x is the doping concentration, where x = 0 is the pure sample MgB_2. The black curve in Figure 5a is the normalized *R-T* curve of the pure MgB_2 sample, and the results show that the *Tc* of the pure MgB_2 sample is 37.4–38.2 K. The other six curves correspond to the *R-T* curve of MgB_2 sample doped with the p-n junction, and the results show that the T_C corresponding to these six doped samples are 36.8–38 K, 37.4–38.4 K, 37.6–39 K, 37.8–38.8 K, 38–38.7 K and 37.2–38.4 K, respectively. The test results show that at low dopant concentrations, such as 0.5 wt.%, the inhomogeneous phases reduce the T_C of the MgB_2 samples ($\Delta T_C < 0$) [56,57]. However, when the dopant concentration reaches a certain value, such as 0.8 wt.%, the inhomogeneous phase enhancement effect occurs, and *Tc* exceeds the pure sample ($\Delta Tc > 0$). When the dopant concentration is 0.9 wt.%, ΔT reaches an increased maximum value of 0.8 K and continues to increase the content of the inhomogeneous phase, while ΔT decreases instead. The characteristics are the same as those of the previous oxide inhomogeneous phase doping results [43,46].

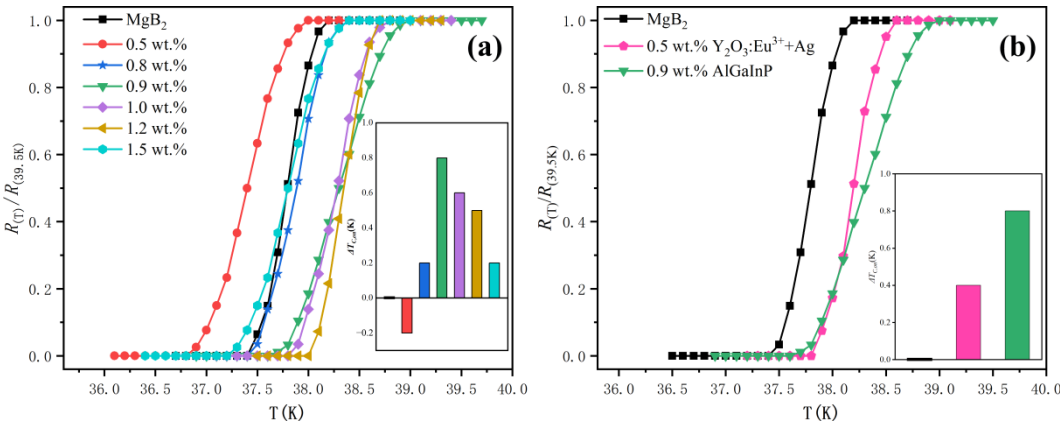

Figure 5. *R-T* curve of MgB_2 sample. (**a**) Doping results of pure MgB_2 and inhomogeneous phase at different concentrations, Insets: the values of ΔT_C ($\Delta T_c = T_c - T_{cpure}$). (**b**) Comparison of the maximum variation of ΔT_C produced by pure MgB_2 and oxide electroluminescence inhomogeneous phase [46], p-n junction inhomogeneous phase.

Figure 6 shows the relationship between J_C and the temperature of the pure MgB_2 and p-n junction with different doping concentrations, which is determined by *I-V* measurement. It can be seen from Figure 6a that J_C of pure MgB_2 and the doped samples decreases with the increase of temperature, which is consistent with the results in literature [34,58,59]. J_C of pure MgB_2 is 8.5×10^4 A/cm² at 20 K, which is comparable to literature [60,61]. At this time, the J_C of the 0.9 wt.% luminescent inhomogeneous phase doped sample is 8.83×10^4 A/cm². When the temperature is low, J_C decreases slowly, and with the increase of temperature, the speed accelerates. The doping of the electroluminescence inhomogeneous phase increases J_C, when $T = 36$ K, J_C of samples with doping concentration of 0.9 wt.% is 37% higher than that of pure MgB_2. When the inhomogeneous phase concentration is 0.5 wt.%, J_C of the sample decreases to a minimum value faster than pure MgB_2; and the samples with higher inhomogeneous phase concentration can have J_C at a higher temperature. For example, J_C of pure MgB_2 was reduced to a minimum at 38.2 K, J_C of the 0.9 wt.% doped sample was reduced to a minimum at 39 K, and J_C of the 1.2 wt % doped sample was reduced to a minimum at 38.7 K.

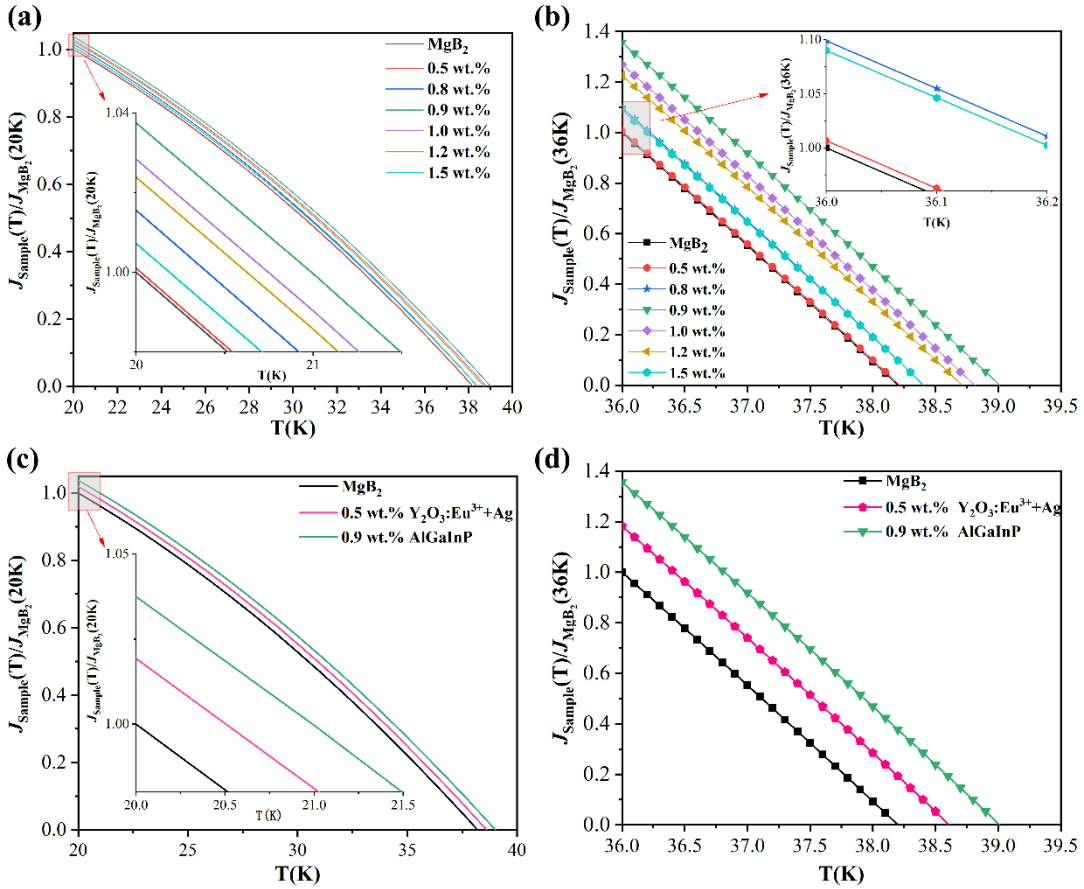

Figure 6. Relationship between J_C and temperature T of MgB_2 samples. (**a**,**b**) Pure MgB_2 and inhomogeneous phase samples. (**c**,**d**) Comparison of J_C for the maximum variation of T_C produced by pure MgB_2 and oxide luminescent inhomogeneous phase [46], p-n junction inhomogeneous phase.

Figure 7 shows the DC magnetization data of pure MgB_2 and MgB_2 mixed with the inhomogeneous phase. The vertical axis shows the complete diamagnetism change of the material, and the Meissner effect of all samples can be observed through the DC magnetization data. With the increase of temperature, complete diamagnetism, or the Meissner effect weakens and eventually disappears, which is consistent with literature [62–64]. The Meissner effect of pure MgB_2 samples disappeared at 37.4 K, and that of the 0.5 wt.% inhomogeneous phase MgB_2 samples disappeared at 36.8 K. The Meissner effect of 0.9 wt.%, 1.0 wt.% and 1.2 wt.% MgB_2 samples disappeared when the temperature was higher than 37.6 K, 37.8 K and 38 K, respectively. It can be seen that the diamagnetic property of the inhomogeneous phase samples with higher concentration is greatly improved compared with that of pure MgB_2. For example, the Meissner effect of the 0.9 wt.% and 1.2 wt.% of the inhomogeneous phase doped MgB_2 samples was increased, compared with that of pure MgB_2. The superconductivity of MgB_2 doped with 1.5 wt.%, 0.9 wt.%, 1.0 wt.%, 1.2 wt.% AlGaInP were similar. Because the superconductivity of samples with the concentrations of 1.5 wt.% and 0.8 wt.% are very close, they are not marked here.

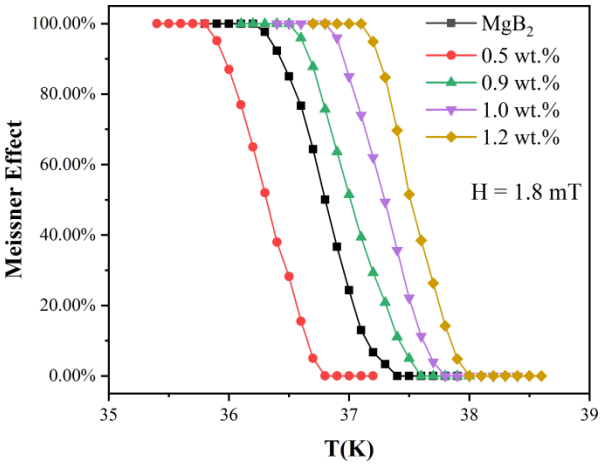

Figure 7. DC magnetization data of pure MgB_2 and MgB_2 doped with inhomogeneous phase.

It can be seen that the p-n junction inhomogeneous phase can produce exactly the same effect as the rare earth oxide inhomogeneous phase. Figure 5b critical transition temperature and Figure 6c,d critical current intensity indicate that the p-n junction inhomogeneous phase's behavior is further improved compared with that of the rare earth oxide inhomogeneous phase. The main reasons may be:

(1) **The advantages of the inhomogeneous phase of the p-n junction nanostructure** Compared with the previous yttrium oxide inhomogeneous phase, the luminescence intensity and long life of the p-n junction nanostructure are far more than those of the previous electro-induced rare earth luminescence materials (Figure 2), which can ensure the stability of material properties. In addition, the p-n junction nanostructure excitation is easier, with only a few volts of excitation required, not hundreds or even thousands of volts. Thus, the electric field applied by the four-point method for measuring superconductivity can meet the requirement. Recently, the mechanism for increasing T_C has been further explored. Figure 8 shows the Raman spectra for pure MgB_2 and MgB_2 doped with 0.5 wt.% Y_2O_3, 1.2 wt.% AlGaInP, 1.0 wt.% AlGaInP, and 0.9 wt.% AlGaInP. Y_2O_3 is a control dopant with no electroluminescent effect. The black scattered points are the measured data, which can be fitted by the Gaussian equation [65] and the results are shown as the red solid lines. Figure 8a show that the Raman shift (ω) of the main peak in the Raman spectrum of pure MgB_2 is 579.2 cm^{-1}, which corresponds to the E_{2g} phonon mode in MgB_2, and the linewidth (γ) is 199.1 cm^{-1}. The measurements are consistent with the results reported in other literature [66–69]. After doping with 0.5 wt.% Y_2O_3, the ω and γ of the E_{2g} phonon mode are 583.7 cm^{-1} and 175.4 cm^{-1} as shown in Figure 8b. The results show that the doping of Y_2O_3 leads to the hardening of the E_{2g} phonon mode [70–72], which weakens the electron-phonon coupling in the MgB_2 and decreases the T_C to 37.6 K. In contrast, the doping of AlGaInP leads to a decrease of ω and an increase of γ. Such a phenomenon of softening of the E_{2g} phonon mode indicates an enhancement of the electron-phonon coupling in the sample [66,73,74], which is beneficial to the improvement of T_C. The $\omega(\gamma)$ for MgB_2 doped with 1.2 wt.%, 1.0 wt.%, and 0.9 wt.% AlGaInP are 557.3 cm^{-1} (234.1 cm^{-1}), 554.6 cm^{-1} (236.5 cm^{-1}), and 552.4 cm^{-1} (245.2 cm^{-1}), and the corresponding T_C are 38.7 K, 38.8 K, and 39.0 K. T_C increases with the enhancement of the softening effect. These results suggest that the softening of the E_{2g} phonon mode in MgB_2 doped with AlGaInP may be the main reason for the enhancement of T_C. Meanwhile, there are still some problems to be solved, such as how to obtain AlGaInP with a uniform particle size and how to distribute the AlGaInP particles evenly in the sample. We will do further research on these issues and study the mechanism in more detail in the follow-up work.

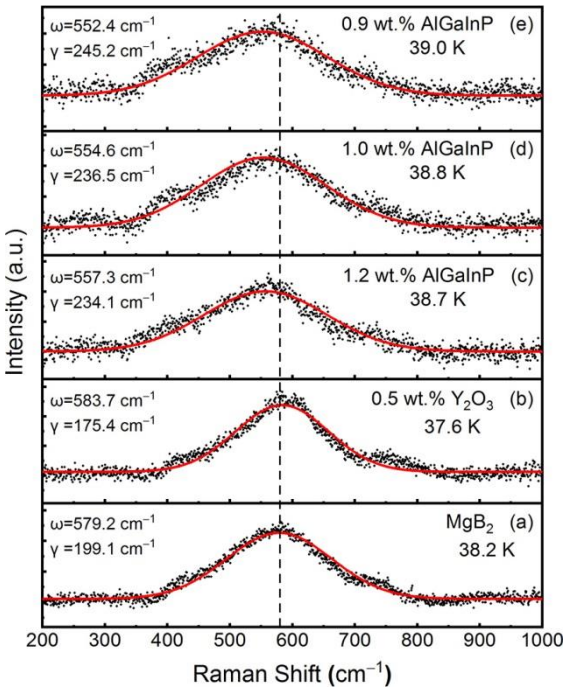

Figure 8. Raman spectra of (**a**) pure MgB_2 and MgB_2 doped with (**b**) 0.5 wt.% Y_2O_3, (**c**) 1.2 wt.% AlGaInP, (**d**) 1.0 wt.% AlGaInP, and (**e**) 0.9 wt.% AlGaInP.

(2) **Performance improvement of smart meta-superconductor** Because the p-n junction inhomogeneous phase exhibits good behavior under external field excitation, the optimal amount of the dopable inhomogeneous phase increases from 0.5 wt.% to 1 wt.% compared with oxide. Thus, the critical temperature *Tc*, current density *Jc* and the Meissner effect of superconductor can be improved compared with the oxide inhomogeneous phase, which provides a wider range for the adjustment of material properties. In particular, the performance stability of the material has been greatly improved, and can be stable for more than several hundred hours. The doping of AlGaInP with too large or too small particle sizes even decreased the T_C of MgB_2. Therefore, selecting AlGaInP with a suitable particle size is also an important factor to improve the T_C. However, AlGaInP particles with a uniform size cannot be obtained by the current preparing process. Improving the preparation process to obtain AlGaInP particles with a uniform size is a focus in our follow-up work.

(3) **The origin of smart superconductivity** In order to explain the above experimental results, we propose an explanatory view of smart superconductivity. Figure 9 shows the schematic diagram of smart superconductivity. By introducing the p-n junction electroluminescent inhomogeneous phase, the photon generated by the inhomogeneous phase in the external field interacts with some superconducting electrons to produce surface plasmon polaritons. The generated evanescent wave can transmit a large number of superconducting electrons with the same energy unimpeded, resulting in the surface plasma system to promote the intense interaction of electrons. The energy injection improves the electron pairing state, promote the superconductivity behavior of the material, increases the critical transition temperature, and forms smart superconductivity.

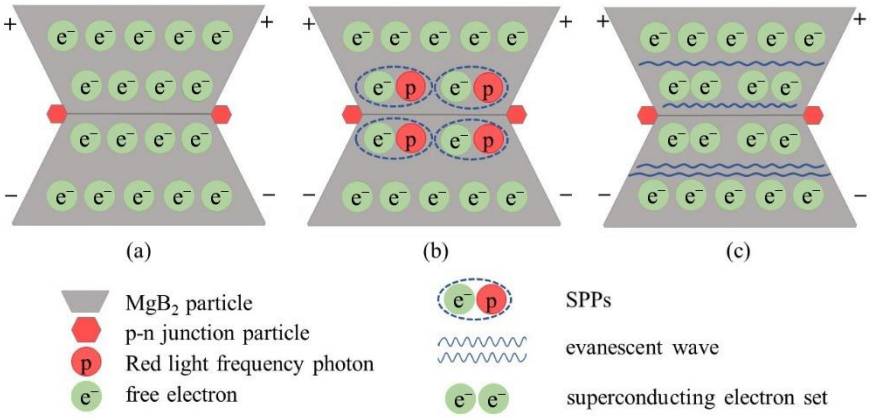

Figure 9. Schematic diagram of smart superconductivity generation. (**a**) Free electrons are uniformly distributed in the superconductor before the measurement field is applied. (**b**) After the measurement electric field is applied, the p-n junction particles in red light wavelength glow and generate a large number of photons. The interaction between photons and some conduction electrons occurs at the particle interface, forming plasmons. (**c**) These surface plasmons propagate as evanescent waves and can transport superconducting electrons. Due to the unimpeded transmission of evanescent wave, the superconductivity of system electrons at higher temperature is promoted.

The conventional superconductor MgB_2 is a standard electroacoustic interaction to form a superconducting transition. It can be seen that before reaching the critical temperature *Tc*, the current density *Jc* (Figure 6) and the diamagnetism *Hc* corresponding to the Meissner effect (Figure 7) of the smart meta-superconductor MgB_2 are both higher than that of pure MgB_2, it is due to the superposition of the electro-acoustic interaction and the SPPs interaction with superconducting electrons. In the experiment, we used two methods of heating and cooling to test. In the heating method, the temperature of the system is reduced to about 10 K first, and then the heating begins. When the temperature exceeds the critical transition temperature of the pure sample, the electro-acoustic interaction fails, but the interaction between the surface plasmas of the smart meta-superconductor and the superconducting electron still exists. Therefore, the critical transition temperature of the smart meta-superconductor MgB_2 is higher than that of the pure MgB_2 superconductor (Figure 5). In the state where *Jc* of the pure MgB_2 superconductor is zero and diamagnetism disappears, *Jc* of the smart meta-superconductor MgB_2 is still non-zero (Figure 6b, d) and diamagnetism still exists (Figure 7). In the cooling method, the system drops from room temperature to 39.1 K, and the initial transition occurs as the temperature continues to drop. The temperature has not reached the critical transition temperature of pure samples of 38.2 K, and the electro-acoustic effect has not yet taken place, but the superconducting transition phenomenon appears, and *Jc* of the smart meta-superconductor MgB_2 also appears. These phenomena confirm that electron-plasmon coupling has been formed, superconducting phase transition has occurred, and smart superconductivity has been achieved. It should be noted that, due to the presence of material resistance, when the temperature reaches a certain point, the interaction between the surface plasmas and the superconducting electrons cannot counteract the effect of material resistance, and superconductivity disappears. However, it is possible to raise the critical transition temperature further by improving the ability of the inhomogeneous phase. Since evanescent waves can exist and transmit at relatively high temperatures, the coupling of superconducting electrons with surface plasmons may promote smart superconductivity at higher temperatures.

Here, we find that the conventional superconductor MgB_2 exhibits smart superconductivity. In fact, in previous studies, we have studied the high-temperature oxide

superconductor, and the smart meta-superconductor can also be formed by doping the rare earth oxide inhomogeneous phase [44,45,47]. Therefore, it can be concluded that they can also show smart superconductivity by the p-n junction nanostructured inhomogeneous phase, and we will provide the research results in the future.

5. Conclusions

In this study, by introducing the p-n junction nanostructured electroluminescent inhomogeneous phase with red wavelength to realize energy injection, the critical transition temperature T_C, the current density J_C and the diamagnetism of the Meissner effect H_C of the smart meta-superconductor MgB_2 are studied. The conclusions are as follows:

(1) The smart meta-superconductor compared with pure MgB_2, the critical transition temperature Tc is increased by 0.8 K, the current density J_C is increased by 37%, and the diamagnetism of the Meissner effect H_C are also significantly improved.

(2) The p-n junction nanostructured inhomogeneous phase has high luminescence intensity, a long stable life and simpler external field requirements. This p-n junction nanostructured inhomogeneous phase SMSCs produces more significant performance changes than the previous yttrium oxide inhomogeneous phase. Under the same conditions, the critical transition temperature ΔT increases by nearly 1 time, and the current density Jc increases significantly.

The coupling between superconducting electrons and SPPs is regarded as an explanation for this phenomenon. The smart meta-superconductor generated by the inhomogeneous phase opens up a new way to improve the performance of superconductors.

Author Contributions: Conceptualization, methodology, X.Z.; software, Q.H., M.S. and H.C.; validation, X.Z., Q.H., M.S. and H.C.; formal analysis, X.Z., H.C. and Y.L.; investigation, Q.H., M.S., H.C., Y.L. and Y.Q.; resources, X.Z.; data curation, H.C., Y.L. and Y.Q., writing—original draft preparation, X.Z.; writing—review and editing, X.Z. and H.C.; visualization, X.Z., Q.H. and M.S.; supervision, X.Z.; project administration, X.Z.; funding acquisition, X.Z. All authors have read and agreed to the published version of the manuscript.

Funding: This research was supported by the National Natural Science Foundation of China for Distinguished Young Scholar under Grant No. 50025207.

Institutional Review Board Statement: Not applicable.

Informed Consent Statement: Not applicable.

Data Availability Statement: The data presented in this study are available on reasonable request from the corresponding author.

Conflicts of Interest: The authors declare no conflicts of interest.

References

1. Gui, X.; Lv, B.; Xie, W.W. Chemistry in Superconductors. *Chem. Rev.* **2021**, *121*, 2966–2991. https://doi.org/10.1021/acs.chemrev.0c00934.
2. Fossheim, K.; Sudbø, A. What is Superconductivity? A Brief Overview. In *Superconductivity: Physics and Applications*; John Wiley & Sons Ltd.: Chichester, UK, 2004; pp. 1–26. https://doi.org/10.1002/0470020784.ch1.
3. DiCarlo, L.; Reed, M.D.; Sun, L.; Johnson, B.R.; Chow, J.M.; Gambetta, J.M.; Frunzio, L.; Girvin, S.M.; Devoret, M.H.; Schoelkopf, R.J. Preparation and Measurement of Three-Qubit Entanglement in a Superconducting Circuit. *Nature* **2010**, *467*, 574–578. https://doi.org/10.1063/1.2807811.
4. Riedinger, R.; Wallucks, A.; Marinković, I.; Lőschnauer, C.; Aspelmeyer, M.; Hong, S.; Grőblacher, S. Remote Quantum Entanglement between Two Micromechanical Oscillators. *Nature* **2018**, *556*, 473–477. https://doi.org/10.1038/s41586-018-0036-z.
5. Bednorz, J.G.; Müller, K.A. Possible high Tc superconductivity in the Ba-La-Cu-O system. *Z. Phys. B Condens. Matter* **1986**, *64*, 189–193. https://doi.org/10.1007/978-94-011-1622-0_32.
6. Mohd Yusuf, N.; Awang Kechik, M.; Baqiah, H.; Soo Kien, C.; Kean Pah, L.; Shaari, A.; Wan Jusoh, W.; Abd Sukor, S.; Mousa Dihom, M.; Talib, Z.; et al. Structural and Superconducting Properties of Thermal Treatment-Synthesised Bulk $YBa_2Cu_3O_{7\delta}$ Superconductor: Effect of Addition of SnO_2 Nanoparticles. *Materials* **2018**, *12*, 92. https://doi.org/10.3390/ma12010092.

7. Kamihara, Y.; Watanabe, T.; Hirano, M.; Hosono, H. Iron-Based Layered Superconductor La[$O_{1-x}F_x$]FeAs (x = 0.05–0.12) with *Tc* = 26 K. *J. Am. Chem. Soc.* **2008**, *130*, 3296–3297. https://doi.org/10.1021/ja800073m.
8. Zhang, P.; Yaji, K.; Hashimoto, T.; Ota, Y.; Kondo, T.; Okazaki, K.; Wang, Z.; Wen, J.; Gu, G.D.; Ding, H.; et al. Observation of topological superconductivity on the surface of an iron-based superconductor. *Science* **2018**, *360*, 182–186. https://doi.org/10.1126/science.aan4596.
9. Drozdov, A.P.; Eremets, M.I.; Troyan, I.A.; Ksenofontov, V.; Shylin, S.I. Conventional superconductivity at 203 kelvin at high pressures in the sulfur hydride system. *Nature* **2015**, *525*, 73–76. https://doi.org/10.1038/nature14964.
10. Cantaluppi, A.; Buzzi, M.; Jotzu, G.; Nicoletti, D.; Mitrano, M.; Pontiroli, D.; Ricco, M.; Perucchi, A.; Di Pietro, P.; Cavalleri, A. Pressure tuning of light-induced superconductivity in K_3C_{60}. *Nat. Phys.* **2018**, *14*, 837–841. https://doi.org/10.1038/s41567-018-0134-8.
11. Drozdov, A.P.; Kong, P.P.; Minkov, V.S.; Besedin, S.P.; Kuzovnikov, M.A.; Mozaffari, S.; Balicas, L.; Balakirev, F.F.; Graf, D.E.; Prakapenka, V.B.; et al. Superconductivity at 250 K in lanthanum hydride under high pressures. *Nature* **2019**, *569*, 528–531. https://doi.org/10.1038/s41586-019-1201-8.
12. Snider, E.; Dasenbrock-Gammon, N.; McBride, R.; Debessai, M.; Vindana, H.; Vencatasamy, K.; Lawler, K.V.; Salamat, A.; Dias, R.P. Room-temperature superconductivity in a carbonaceous sulfur hydride. *Nature* **2020**, *586*, 373–377. https://doi.org/10.1038/s41586-020-2801-z.
13. Fausti, D.; Tobey, R.I.; Dean, N.; Kaiser, S.; Dienst, A.; Hoffmann, M.C.; Pyon, S.; Takayama, T.; Takagi, H.; Cavalleri, A. Light-induced superconductivity in a stripe-ordered cuprate. *Science* **2011**, *331*, 189–191. https://doi.org/10.1126/science.1197294.
14. Cavalleri, A. Photo-induced superconductivity. *Contemp. Phys.* **2017**, *59*, 31–46. https://doi.org/10.1080/00107514.2017.1406623.
15. Bardeen, J.; Cooper, L.N.; Schrieffer, J.R. Theory of Superconductivity. *Phys. Rev.* **1957**, *108*, 1175–1204. https://doi.org/10.1103/PhysRev.108.1175.
16. Bardeen, J. Theory of the Meissner Effect in Superconductors. *Phys. Rev.* **1955**, *97*, 1724–1725. https://doi.org/10.1103/PhysRev.97.1724.
17. Chung, D.Y. The Basic Cause of Superconductivity. *J. Mod. Phys.* **2015**, *6*, 26–36. https://doi.org/10.4236/jmp.2015.61005.
18. Qiu, D.; Gong, C.; Wang, S.; Zhang, M.; Yang, C.; Wang, X.; Xiong, J. Recent Advances in 2D Superconductors. *Adv. Mater.* **2021**, *33*, e2006124. https://doi.org/10.1002/adma.202006124.
19. Nagamatsu, J.; Nakagawa, N.; Muranaka, T.; Zenitani, Y.; Akimitsu, J. Superconductivity at 39 K in magnesium diboride. *Nature* **2001**, *410*, 63–64. https://doi.org/10.1038/35065039.
20. Zhao, Y.G.; Zhang, X.P.; Qiao, P.T.; Zhang, H.T.; Jia, S.L.; Cao, B.S.; Zhu, M.H.; Han, Z.H.; Wang, X.L.; Gu, B.L. Effect of Li doping on structure and superconducting transition temperature of $Mg_{1-x}Li_xB_2$. *Phys. C* **2001**, *361*, 91–94. https://doi.org/10.1016/S0921-4534(01)00907-8.
21. Mackinnon, I.D.R.; Winnett, A.; Alarco, J.A.; Talbot, P.C. Synthesis of MgB_2 at low temperature and autogenous pressure. *Materials* **2014**, *7*, 3901–3918. https://doi.org/10.3390/ma7053901.
22. Ozturk, O.; Asikuzun, E.; Kaya, S.; Koc, N.S.; Erdem, M. The effect of Ar ambient pressure and annealing duration on the cicrostructure, superconducting properties and activation energies of MgB_2 superconductors. *J. Supercond. Nov. Magn.* **2016**, *30*, 1161–1169. https://doi.org/10.1007/s10948-016-3877-4.
23. Cheng, F.; Ma, Z.; Liu, C.; Li, H.; Shahriar, A.; Hossain, M.; Bando, Y.; Yamauchi, Y.; Fatehmulla, A.; Farooq, W.A.; et al. Enhancement of grain connectivity and critical current density in the ex-situ sintered MgB_2 superconductors by doping minor Cu. *J. Alloys Compd.* **2017**, *727*, 1105–1109. https://doi.org/10.1016/j.jallcom.2017.08.152.
24. Grivel, J.C.; Rubešová, K. Increase of the critical current density of MgB_2 superconducting bulk samples by means of methylene blue dye additions. *Phys. C* **2019**, *565*, 1353506. https://doi.org/10.1016/j.physc.2019.1353506.
25. Slusky, J.S.; Rogado, N.; Regan, K.A.; Hayward, M.A.; Khalifah, P.; He, T.; Inumaru, K.; Loureiro, S.M.; Haas, M.K.; Zandbergen, H.W.; et al. Loss of superconductivity with the addition of Al to MgB_2 and a structural transition in $Mg_{1-x}Al_xB_2$. *Nature* **2001**, *410*, 343. https://doi.org/10.1038/35066528.
26. Li, S.Y.; Xiong Y.M.; Mo, W.Q.; Fan, R.; Wang, C.H.; Luo, X.G.; Sun, Z.; Zhang, H.T.; Li, L.; Cao, L.Z.; et al. Alkali metal substitution efffects in $Mg_{1-x}A_xB_2$ (A = Li and Na). *Phys. C.* **2001**, *363*, 219–223. https://doi.org/10.1016/S0921-4534(01)01071-1.
27. Susner, M.A.; Bohnenstiehl, S.D.; Dregia, S.A.; Sumption, M.D.; Yang, Y.; Donovan, J.J.; Collings, E.W. Homogeneous carbon doping of magnesium diboride by high-temperature, high-pressure synthesis. *Appl. Phys. Lett.* **2014**, *104*, 162603. https://doi.org/10.1063/1.4871578.
28. Shahabuddin, M.; Madhar, N.A.; Alzayed, N.S.; Asif, M. Uniform dispersion and exfoliation of multi-walled carbon nanotubes in CNT- MgB_2 superconductor composites using surfactants. *Materials* **2019**, *12*, 3044. https://doi.org/10.3390/ma12183044.
29. Tang, S.P.;Wang, D.L.; Zhang, X.P.; Zhang, Q.J.; Li, C.; Ma, Y.W.; Oguro, H.; Awaji, S.; Watanabe, K. Improved Transport J_C in MgB_2 Tapes by Graphene Doping. *J. Supercond. Nov. Magn.* **2014**, *27*, 2699–2705. https://doi.org/10.1007/s10948-014-2804-9.
30. Annabi, M.; M'Chirgui, A.; Ben Azzouz, F.; Zouaoui, M.; Ben Salem, M. Addition of nanometer Al_2O_3 during the final processing of (Bi,Pb)-2223 superconductors. *Phys. C Supercond.* **2004**, *405*, 25–33. https://doi.org/10.1016/j.physc.2004.01.012.
31. Hua, L.; Yoo, J.; Ko, J.; Kim, H.; Chung, H.; Qiao, G. Microstructure and phase evolution of ultrafine MgO doped Bi-2223/Ag tapes. *Phys. C Supercond.* **1997**, *291*, 149–154. https://doi.org/10.1016/S0921-4534(98)00002-1.
32. Ahmad, I.; Sarangi, S.N.; Sarun, P.M. Enhanced critical current density and flux pinning of anthracene doped magnesium diboride superconductor. *J. Alloys Compd.* **2021**, *884*, 160999. https://doi.org/10.1016/j.jallcom.2021.160999.

33. Abbasi, H.; Taghipour, J.; Sedghi, H. Superconducting and transport properties of (Bi–Pb)–Sr–Ca–Cu–O with Cr_2O_3 additions. *J. Alloys Compd.* **2010**, *494*, 305–308. https://doi.org/10.1016/j.jallcom.2010.01.018.
34. Shelby, R.A.; Smith, D.R.; Schultz, S. Experimental verification of a negative index of refraction. *Science* **2001**, *292*, 77–79. https://doi.org/10.1016/s0002-9394(01)01173-4.
35. Zhao, X.P. Bottom-up fabrication methods of optical metamaterials. *J. Mater. Chem.* **2012**, *22*, 9439–9449. https://doi.org/10.1039/C2JM15979A.
36. Smolyaninov, I.I.; Smolyaninova, V.N. Is There a Metamaterial Route to High Temperature Superconductivity? *Adv. Condens. Matter Phys.* **2014**, *2014*, 479635. https://doi.org/10.1155/2014/479635.
37. Smolyaninova, V.N.; Yost, B.; Zander, K.; Osofsky, M.S.; Kim, H.; Saha, S.; Greene, R.L.; Smolyaninov, I.I. Experimental demonstration of superconducting critical temperature increase in electromagnetic metamaterials. *Sci. Rep.* **2014**, *4*, 7321. https://doi.org/10.1038/srep07321.
38. Smolyaninov, I.I.; Smolyaninova, V.N. Theoretical modeling of critical temperature increase in metamaterial superconductors. *Phys. Rev. B* **2016**, *93*, 184510. https://doi.org/10.1103/PhysRevB.93.184510.
39. Zhang, Z.W.; Tao, S.; Chen, G.W.; Zhao, X.P. Improving the Critical Temperature of MgB_2 Superconducting Metamaterials Induced by Electroluminescence. *J. Supercond. Nov. Magn.* **2016**, *29*, 1159–1162. https://doi.org/10.1007/s10948-015-3344-7.
40. Tao, S.; Li, Y.B.; Chen, G.W.; Zhao, X.P. Critical Temperature of Smart Meta-superconducting MgB_2. *J. Supercond. Nov. Magn.* **2017**, *30*, 1405–1411. https://doi.org/10.1007/s10948-016-3963-7.
41. Li, Y.B.; Chen, H.G.; Qi, W.C.; Chen, G.W.; Zhao, X.P. Inhomogeneous Phase Effect of Smart Meta-Superconducting MgB_2. *J. Low Temp. Phys.* **2018**, *191*, 217–227. https://doi.org/10.1007/s10909-018-1865-8.
42. Chen, H.G.; Li, Y.B.; Chen, G.W.; Xu, L.X.; Zhao, X.P. The Effect of Inhomogeneous Phase on the Critical Temperature of Smart Meta-superconductor MgB_2. *J. Supercond. Nov. Magn.* **2018**, *31*, 3175–3182. https://doi.org/10.1007/s10948-018-4599-6.
43. Li, Y.B.; Chen, H.G.; Wang, M.Z.; Xu, L.X.; Zhao, X.P. Smart meta-superconductor MgB_2 constructed by the dopant phase of luminescent nanocomposite. *Sci. Rep.* **2019**, *9*, 14194. https://doi.org/10.1038/s41598-019-50663-6.
44. Chen, H.G.; Li, Y.B.; Wang, M.Z.; Han, G.Y.; Shi, M.; Zhao, X.P. Smart metastructure method for increasing T_C of Bi(Pb)SrCaCuO high-temperature superconductors. *J. Supercond. Nov. Magn.* **2020**, *33*, 3015–3025. https://doi.org/10.1007/s10948-020-05591-2.
45. Chen, H.G.; Wang, M.Z.; Qi, Y.; Li, Y.B.; Zhao, X.P. Relationship between the T_C of Smart Meta-Superconductor Bi(Pb)SrCaCuO and Inhomogeneous Phase Content. *Nanomaterials* **2021**, *11*, 1061. https://doi.org/10.3390/nano11051061.
46. Li, Y.B.; Han, G.Y.; Zou, H.Y.; Tang, L.; Chen, H.G.; Zhao, X.P. Reinforcing Increase of ΔT_C in MgB_2 Smart Meta-Superconductors by Adjusting the Concentration of Inhomogeneous Phases. *Materials* **2021**, *14*, 3066. DOI: 0.3390/ma14113066.
47. Chen, H.G.; Li, Y.B.; Qi, Y.; Wang, M.Z.; Zou, H.Y.; Zhao, X.P. Critical Current Density and Meissner Effect of Smart Meta-Superconductor MgB_2 and Bi(Pb)SrCaCuO. *Materials* **2022**, *15*, 972. https://doi.org/10.3390/ma15030972.
48. Ye, J.T.; Inoue, S.; Kobayashi, K.; Kasahara, Y.; Yuan, H.T.; Shimotani, H.; Iwasa, Y. Liquid-gated interface superconductivity on an atomically flat film. *Nature Mater.* **2010**, *9*, 125–128. https://doi.org/10.1038/nmat2587.
49. Kouji, T.; Akiyo, M.; Hidekazu, S.; Hidenori, T. Electric-field-induced superconductivity at 9.4 K in a layered transition metal disulphide MoS_2. *Appl. Phys. Lett.* **2012**,*101*, 042603. https://doi.org/10.1063/1.4740268.
50. Chen, G.W.; Qi, W.C.; Li, Y.B.; Yang, C.S.; Zhao, X.P. Hydrothermal synthesis of Y_2O_3:Eu^{3+} nanorods and its growth mechanism and luminescence properties. *J. Mater. Sci. Mater. Electron.* **2016**, *27*, 5628–5634. https://doi.org/10.1007/s10854-016-4470-0.
51. Wang, M.Z.; Xu, L.X.; Chen, G.W.; Zhao, X.P. Topological luminophor Y_2O_3:Eu^{3+}+Ag with high electroluminescence performance. *ACS Appl. Mater. Interfaces* **2019**, *11*, 2328–2335. https://doi.org/10.1021/acsami.8b20046.
52. Sunwong, P.; Higgins, J.S.; Tsui, Y.; Raine, M.J.; Hampshire, D.P. The critical current density of grain boundary channels in polycrystalline HTS and LTS superconductors in magnetic fields. *Supercond. Sci. Technol.* **2013**, *26*, 095006. https://doi.org/10.1088/0953-2048/26/9/095006.
53. Rakshit, D.; Sk, T.; Das, P.; Haldar, S.; Ghosh, A.K. Exponential reduction in critical current density in Eu1-xCexBa2Cu3O7-_superconductors near critical temperature. *Phys. C Supercond.* **2021**, *588*, 1353909. https://doi.org/10.1016/j.physc.2021.1353909.
54. Tampieri, A.; Fiorani, D.; Sparvieri, N.; Rinaldi, S.; Celotti, G.; Bartolucci, R. Granular and intergranular properties of hot pressed BSCCO (2223) superconductors. *J. Mater. Sci. Mater. Electron.* **1999**, *34*, 6177–6182. https://doi.org/10.1023/A:1004786324179.
55. Sunshine, S.A.; Siegrist, T.; Schneemeyer, L.F.; Murphy, D.W.; Cava, R.J.; Batlogg, B.; Van Dover, R.B.; Fleming, R.M.; Glarum, S.H.; Nakahara, S.; et al. Structure and physical properties of single crystals of the 84-K superconductor $Bi_{2.2}Sr_2Ca_{0.8}Cu_2O_{8+\delta}$. *Phys. Rev. B* **1988**, *38*, 893–896. https://doi.org/10.1103/PhysRevB.38.893.
56. Dou, S.X.; Soltanian, S.; Horvat, J.; Wang, X.L.; Zhou, S.H.; Ionescu, M.; Liu, H.K.; Munroe, P.; Tomsic, M. Enhancement of the critical current density and flux pinning of MgB_2 superconductor by nanoparticle SiC doping. *Appl. Phys. Lett.* **2002**, *81*, 3419–3421. https://doi.org/10.1063/1.1517398.
57. Batalu, A.; Stanciuc, M.; Moldovan, L.; Aldica, G.; Badica, P. Evaluation of pristine and Eu_2O_3-added MgB_2 ceramics for medical applications: Hardness, corrosion resistance, cytotoxicity and antibacterial activity. *Mater. Sci. Eng. C* **2014**, *42*, 350–361. https://doi.org/10.1016/j.msec.2014.05.046.

58. Buzea, C.; Yamashita, T. Review of superconducting properties of MgB_2. *Supercond. Sci. Technol*. **2001**, *14*, R115–R146. https://doi.org/10.1088/0953-2048/14/11/201.
59. Zhang, H.; Zhao, Y.; Zhang, Y. The Effects of Excess Mg Addition on the Superconductivity of MgB_2. *J. Supercond. Nov. Magn*. **2015**, *28*, 2711–2714. https://doi.org/10.1007/s10948-015-3120-8.
60. Arvapalli, S.S.; Miryala, M.; Jirsa, M.; Murakami, M. Size reduction of boron particles by high-power ultrasound for optimization of bulk MgB_2. *Supercond. Sci. Technol*. **2020**, *33*, 115009. https://doi.org/10.1088/1361-6668/abb63e.
61. Peng, J.M.; Cai, Q.; Cheng, F.; Ma, Z.Q.; Li, C.; Xin, Y.; Liu, Y.C. Enhancement of critical current density by a "MgB_2-MgB_4" reversible reaction in self-sintered ex-situ MgB_2 bulks. *J. Alloys Compd.* **2017**, *694*, 24–29. https://doi.org/10.1016/j.jallcom.2016.09.312.
62. Krishna, N.M.; Lingam, L.S.; Ghosh, P.K.; Shrivastava, K.N. Effect of current-loop sizes on the para-Meissner effect in superconductors. *Phys. C Supercond.* **1998**, *294*, 243–248. https://doi.org/10.1016/S0921-4534(97)01738-3.
63. Posselt, H.; Muller, H.; Andres, K.; Saito, G. Reentrant Meissner effect in the organic conductor κ-(BEDT-TTF)$_2$Cu[N(CN)$_2$]Cl under pressure. *Phys. Rev. B* **1994**, *49*, 15849–15852. https://doi.org/10.1103/PhysRevB.49.15849.
64. Horiuchi, T.; Kawai, T.; Kawai, S.; Ogura, K. The trial of making Bi-Sr-Ca-Cu-M-O superconductors (M = Li, Na, K, Rb, Cs). *Ferroelectrics* **1990**, *109*, 351–356. https://doi.org/10.1080/00150199008211438.
65. Sakuntala, T.; Bharathi, A.; Deb, S.K.; Gayathri, N.; Sundar, C.S.; Hariharan, Y. Raman scattering investigation of electron–phonon coupling in carbon substituted MgB_2. *J. Phys. Condens. Matter* **2005**, *17*, 3285–3292. https://doi.org/10.1088/0953-8984/17/21/021.
66. Bohnen, K.P.; Heid, R.; Renker, B. Phonon dispersion and electron-phonon coupling in MgB_2 and AlB_2. *Phys. Rev. Lett.* **2001**, *86*, 5771–5774. https://doi.org/10.1103/PhysRevLett.86.5771.
67. Postorino, P.; Congeduti, A.; Dore, P.; Nucara, A.; Bianconi, A.; Di Castro, D.; De Negri, S.; Saccone, A. Effect of the Al content on the optical phonon spectrum in $Mg_{1-x}Al_xB_2$. *Phys. Rev. B* **2001**, *65*, 020507. https://doi.org/10.1103/physrevb.65.020507.
68. Renker, B.; Bohnen, K.B.; Heid, R.; Ernst, D.; Schober, H.; Koza, M.; Adelmann, P.; Schweiss, P.; Wolf, T. Strong renormalization of phonon frequencies in $Mg_{1-x}Al_xB_2$. *Phys. Rev. Lett.* **2002**, *88*, 067001. https://doi.org/10.1103/PhysRevLett.88.067001.
69. Li, W.X.; Zeng, R.; Lu, L.; Dou, S.X. Effect of thermal strain on J_c and T_c in high density nano-SiC doped MgB_2. *J. Appl. Phys.* **2011**, *109*, 07E108. https://doi.org/10.1063/1.3549590.
70. Goncharov, A.F.; Struzhkin, V.V. Pressure dependence of the Raman spectrum, lattice parameters and superconducting critical temperature of MgB_2: Evidence for pressure-driven phonon-assisted electronic topological transition. *Phys. C* **2003**, *385*, 117–130. https://doi.org/10.1016/S0921-4534(02)02311-0.
71. Arvanitidis, J.; Papagelis, K.; Prassides, K.; Kourouklis, G.A.; Ves, S.; Takenobu, T.; Iwasa, Y. Raman spectroscopic study of carbon substitution in MgB_2. *J. Phys. Chem. Solids* **2004**, *65*, 73–77. https://doi.org/10.1016/j.jpcs.2003.08.010.
72. Masui, T.; Lee, S.; Tajima, S. Carbon-substitution effect on the electronic properties of MgB_2 single crystals. *Phys. Rev. B* **2004**, *70*, 024504. https://doi.org/10.1103/PhysRevB.70.024504.
73. Pogrebnyakov, A.V.; Redwing, J.M.; Raghavan, S.; Vaithyanathan, V.; Schlom, D.G.; Xu, S.Y.; Li, Q.; Tenne, D.A.; Soukiassian, A.; Xi, X.X.; et al. Enhancement of the superconducting transition temperature of MgB_2 by a strain-induced bond-stretching mode softening. *Phys. Rev. Lett.* **2004**, *93*, 147006. https://doi.org/10.1103/PhysRevLett.93.147006.
74. Li, W.X.; Xu, X.; De Silva, K.S.B.; Xiang, F.X.; Dou, S.X. Graphene Micro-Substrate Induced High Electron-Phonon Coupling in MgB_2. *IEEE. T. Appl. Supercon.* **2013**, *23*, 7000104. https://doi.org/10.1109/tasc.2012.2231139.